Iranian Journal of Fuzzy Systems

Volume 23, Number 3, (2026), pp. 31-50

Original paper

University of Sistan and Baluchestan

Design of a two-layer adaptive gain scheduling Type-II fuzzy logic controller for improved seismic resilience in multistory structures

M. R. Kamali Ardakani [1], S. R. Khaledi [2] and M. Pourgholi [3]

[1] *Faculty of Automation Engineering, University of Bologna, Italy, Bologna*
[2] *Faculty of Bioinformatics, University of Bologna, Italy, Bologna*
[3] *Faculty of Electrical Engineering, Shahid Beheshti University, Tehran, Iran*

mohammadreza.kamali@studio.unibo.it, sajja.rezvanikhaledi@studio.unibo.it, m_pourgholi@sbu.ac.ir

Abstract

This study introduces a novel Two-Layer Type-II Adaptive Fuzzy Logic Controller (2LT2-FLC) to enhance seismic resilience in structural engineering. The innovative dual-layer approach integrates an inner adaptive fuzzy layer, which dynamically adjusts input scaling gains in real-time based on the instantaneous range of structural response, with a core fuzzy layer that employs interpretable IF-THEN rules to compute control forces. This design overcomes the limitations of controllers with static parameters by providing continuous self-adaptation to varying seismic excitation levels. The controller's performance was evaluated on a nonlinear four-story steel frame benchmark model, with parameters validated against established structural dynamics literature, under historical earthquake records (Kobe and Northridge). The proposed 2LT2-FLC significantly reduced peak inter-story drift—by 50.18% on the second floor and 47.69% on the fourth floor during the Kobe earthquake—outperforming both Type-II Fuzzy-PID and ANFIS-PID controllers. The controller operates with an average computation time of approximately 0.2 milliseconds per time step, confirming its suitability for real-time applications. By simplifying real-time adaptation for nonlinear systems, the 2LT2-FLC ensures robust, interpretable, and computationally efficient control, presenting a significant advancement for practical seismic mitigation.

Keywords: Type-2 fuzzy logic controller, CGO optimization, ANFIS-PID, fuzzy-PID.

1 Introduction

Modern engineering faces the challenge of modeling increasingly complex systems, where simplifying assumptions often introduce uncertainties that compromise accuracy. Fuzzy controllers, including Type-I and Type-II variants, have emerged as powerful tools to address these uncertainties. Type-I fuzzy controllers effectively manage low-level uncertainties but are limited by their reliance on crisp membership function outputs, which restricts their ability to handle highly uncertain systems. In contrast, Type-II fuzzy controllers employ interval-based membership outputs with secondary membership degrees, enabling them to better capture complex uncertainties. However, designing effective fuzzy controllers remains challenging, particularly in defining appropriate rules and optimizing membership function placement. Incorrect rule formulation can lead to erroneous outputs, requiring expert system knowledge. Additionally, the static nature of membership functions, typically predefined within fixed ranges, poses a persistent issue. While modern optimization techniques can adjust these functions, their application in real-time systems is hindered by computational constraints and system-specific parameter requirements. Real-time control demands rapid responses, rendering traditional optimization methods impractical for dynamic environments. This article proposes a Two-Layer Type-II Adaptive Fuzzy Logic Controller that enables online adjustment of membership function placement, enhancing the adaptability of fuzzy controllers for real-world applications. The proposed method was tested on a nonlinear structural

Corresponding Author: M. Pourgholi
Received: June 2025; Revised: January 2026; Accepted: May 2026.
https://doi.org/10.22111/ijfs.2026.52466.9253

model, focusing on seismic resilience—a critical challenge in modern structural and civil engineering. Seismic resilience involves designing control systems to mitigate earthquake-induced vibrations in buildings and infrastructures. Traditional passive devices, such as fixed tuned mass dampers (TMDs) and base isolators, have shown limitations due to their inability to adapt to the unpredictable intensity and frequency of earthquakes [4].

1.1 Evolution of seismic control strategies

Early seismic control relied heavily on passive devices like TMDs, tuned liquid dampers (TLDs), and tuned liquid column dampers (TLCDs). In an experimental study [4], researchers compared the damping performance of these devices on a scaled three-story steel structure under dynamic loading. Their findings showed that TMDs achieved the greatest damping effect (59.9% at a 1.8 kg mass), followed by TLCDs (50.6%) and TLDs (46.9%). While all systems reduced peak displacements by 15–17%, their effectiveness depended on precise mass and frequency tuning, highlighting the need for more adaptive solutions. A significant advancement came with the integration of fuzzy logic and genetic algorithms (GAs). Authors in [15] demonstrated that combining fuzzy logic with GAs could enhance vibration suppression in flexible structures. By encoding control rules in linguistic form and evolving membership functions and rule weights via GA search, they achieved up to a 30% reduction in peak response compared to fixed-gain controllers. This work underscored the potential of soft-computing strategies to address structural nonlinearities and uncertainties. Building on this foundation, Wang and Lin [19] applied fuzzy logic to the seismic control of a 40-story steel moment frame, using story drift and drift rate as inputs. Their study reported 25–35% reductions in roof displacement and inter-story drift under El-Centro and Kobe earthquake records. Their use of multiple fuzzy inputs aligned with the building's vibration patterns, suggesting the future need for layered or multi-level fuzzy systems. However, their membership functions required manual tuning and could not adapt automatically during strong earthquakes, a challenge later addressed through automated optimization. In [13], authors extended evolutionary optimization to high-rise structures equipped with active mass dampers. Using GAs to tune membership function shapes and the weights of over 25 rules, they achieved up to 45% reductions in base shear and 40% decreases in top-floor acceleration under Northridge and Kobe earthquakes. This paper [13] investigates seismic vibration mitigation in a high-rise structure by employing an Active Tuned Mass Damper (ATMD) governed by a fuzzy logic control strategy. The controller is formulated using top-story displacement and velocity as feedback signals, while a genetic algorithm is utilized to optimally tune the fuzzy membership functions, rule base weighting, and key ATMD design parameters such as mass, frequency, and damping ratios. Performance is evaluated on an 11-story shear building model subjected to several historical earthquake records, and the proposed GA-optimized fuzzy control framework is benchmarked against both a passive tuned mass damper and a classical LQR controller. The simulation results indicate that the optimized fuzzy approach yields the most substantial reduction in peak structural responses—particularly at the top floor—although this improvement is typically accompanied by higher required control forces compared with LQR.

1.2 Advances in intelligent control

Over the past decade, fuzzy logic-based control methods, including Fuzzy Logic Controllers (FLCs), Type-II FLCs, Fuzzy-PID, and Adaptive Neuro-Fuzzy Inference Systems (ANFIS), have shown promise in handling the nonlinearity and uncertainties of structural dynamics. Unlike passive systems, these intelligent methods naturally accommodate the unpredictable nature of earthquake responses. Fuzzy logic's ability to integrate with PID controllers and neural networks, as in Fuzzy-PID and ANFIS-PID, has further enhanced its applicability. Researchers in [10] employed an Interval Type-II Fuzzy Logic Controller (IT2FLC) with an ATMD for the seismic control of an 11-story shear building. This work considered soil–structure interaction (SSI), a factor often overlooked in ideal control studies. The IT2FLC demonstrated superior robustness compared to Type-I FLC under uncertain and nonlinear SSI conditions, achieving over 40% reductions in roof displacement and inter-story drift, with amplified improvements under soft soil conditions. However, IT2FLCs face higher computational complexity and type-reduction overhead, limiting their real-time feasibility in hardware-embedded systems. Another study [5] explored GA-optimized ANFIS controllers for a semi-active system with magnetorheological (MR) dampers. Targeting an 11-story steel frame under multiple earthquake records (El Centro, Kobe, Hachinohe, and Northridge), the ANFIS-GA controller outperformed linear quadratic regulator (LQR), clipped-optimal control, and fixed fuzzy controllers, achieving 30–44% lower relative displacement and inter-story drift. Despite its success, ANFIS relies on offline training and lacks transparent rule interpretation. In [18], researchers compared ANFIS-PID, Fuzzy-PID, and classical PID controllers for the seismic control of 3- and 5-story buildings using MR dampers. Tested under Gadha (1997), Kobe (1995), and Northridge (1994) earthquake records, the ANFIS-PID configuration outperformed both PID and Fuzzy-PID in displacement and acceleration reduction. However, these hybrid methods relied on pre-trained ANFIS systems or fixed fuzzy rule sets, unlike the proposed architecture,

which introduces online adaptive gain tuning to enhance resilience against unexpected or multi-modal excitations.

1.3 Optimizing classical and intelligent control

While intelligent controllers have advanced, some research has focused on optimizing classical methods. In [2], authors proposed multi-objective tuned PID controllers using the Non-dominated Sorting Genetic Algorithm II (NSGA-II). Compared with LQR controllers on an 11-story building with an ATMD under four strong ground motions, the tuned PID controllers minimized roof displacement and inter-story drift more effectively while using fewer sensors. However, PID controllers lack the inherent nonlinearity handling and linguistic flexibility of fuzzy systems and do not adapt during runtime. Recent studies have extended intelligent control to complex scenarios, such as coupled structures and base-isolated systems. In [1], researchers developed an ANFIS-based semi-active control system (FLC-DV) for a coupled wall system with MR dampers. Tested under El Centro, Hachinohe, and Kobe earthquakes, the system significantly reduced peak displacements and inter-story drift in both the isolated building and the coupled wall. However, it relied on offline ANFIS training, limiting rule interpretability. In another study [7] researchers addressed pulse-type near-field ground motions using a Pareto-optimized FLC-ATMD system for a 15-story 3D building model. By jointly optimizing FLC parameters and ATMD characteristics with a multi-objective algorithm, they achieved up to 50% reduction in displacement compared to uncontrolled structures. However, the architecture was fixed during runtime. Researchers in [8] explored dual actively controlled TMDs (MATMDs) on an 11-story building. Using fuzzy logic controllers, the study evaluated different mass distributions under long- and short-period earthquake excitations, achieving 10–15% improved vibration reduction over single-damper configurations. However, the static nature of logic and gain parameters limit adaptability. Authors in [3] used an Upgraded Whale Optimization Algorithm (UWOA) to search for optimal fuzzy parameters in a nonlinear steel frame, achieving 10–15% improvements over GA-based tuning. However, UWOA remained an offline method, unable to adapt gains in real time. Fathi et al. [9] proposed an adaptive two-layer Type-1 fuzzy logic controller for seismic vibration reduction, in which membership functions are updated online using structural acceleration data and the Slime Mould Algorithm is used to optimize controller gains. The controller was evaluated on a four-story steel frame under near-field and far-field earthquake excitations, achieving up to 44% reduction in top-floor displacement. Although the method improves adaptability compared with fixed-range Type-1 fuzzy controllers, it still depends on SMA-based gain optimization and does not incorporate Type-II uncertainty modeling. In [14] introduced Active Disturbance Rejection Control (ADRC) as a model-independent alternative, achieving 20% lower floor accelerations than LQR or PID. However, ADRC's sensitivity to sensor noise highlights the advantage of rule-based fuzzy gain scheduling. In this regard, researchers in [20] used a Modified Black Hole Optimization (MBHO) algorithm to tune PID gains in real time, achieving 30% better performance than standard PID. Researcher designed a robust anti-windup PID scheme [21] that improved vibration suppression by preventing integrator saturation but struggled with structural nonlinearity and multi-modal excitation, areas where the layered fuzzy approach excels. Sabetahd and Jafarzadeh recently proposed an adaptive chaotic fuzzy neural network controller for an 11-story building equipped with an ATMD [11]. Their strategy is built upon interval type-2 fuzzy systems, where a multilayer perceptron neural network is used to estimate the system dynamics and Jacobian, and the controller parameters are updated online via a combination of error backpropagation and an Extended Kalman filter. An additional adaptive IT2 fuzzy neural network compensator and an optimized simple adaptive controller, tuned through an improved grey wolf optimization algorithm, are also incorporated. Their results show that the adaptive chaotic fuzzy neural network controller can significantly reduce maximum displacement, inter-story drift, base shear, and acceleration, outperforming several contemporary control strategies under seismic uncertainties. A critical analysis of the studies reveals a common constraint: reliance on offline design and optimization. Whether through evolutionary algorithms, neurofuzzy training, or expert tuning, the parameters of these controllers—membership functions, rule consequents, gains—remain static during operation. This inherently limits their adaptability to seismic events whose intensity and frequency content may deviate significantly from the design basis. The proposed Two-Layer Type-II Adaptive Fuzzy Logic Controller (2LT2-FLC) is designed to bridge this gap. Its innovation lies in an inner adaptive layer that performs real-time gain scheduling. This layer dynamically adjusts the input scaling based on the instantaneous response of the structure, ensuring the core fuzzy controller always operates on a normalized input signal. This architecture provides a fundamental shift from offline-adjusted controllers to those capable of self-adaptation during runtime, offering robust performance across a wide and unforeseen range of seismic excitations.

1.4 The two-layer fuzzy logic controller

The proposed two-layer interval type-II fuzzy logic controller (2LT2-FLC) addresses the limitations of fixed-range fuzzy controllers by separating online input normalization from the core rule-based control law. Specifically, an inner adaptive

fuzzy layer performs real-time gain scheduling by updating the input scaling factors according to the instantaneous range of the measured structural response (error and error derivative). The outer (core) interval type-2 fuzzy controller then operates on normalized signals within a fixed domain, enabling a compact and interpretable rule base to generate the control force. This separation preserves the transparency of IF–THEN rules while improving robustness across different earthquake intensity levels and frequency contents.

In contrast to metaheuristic tuning methods that require iterative optimization, the proposed adaptation mechanism is lightweight during execution and does not rely on repeated online search procedures. Consequently, it is well-suited for real-time implementation and is less sensitive to system-specific tuning compared with controllers whose performance strongly depends on an optimized parameter set. In addition, unlike ANFIS-based controllers, the proposed method does not require data-driven training, reducing the risk of overfitting to a particular dataset.

The main contributions of this paper are summarized as follows:

I. A two-layer interval type-2 fuzzy control architecture in which an inner adaptive layer performs real-time gain scheduling to keep the inputs of the core fuzzy controller normalized.

II. A bounded analysis showing that the scaled inputs of the core fuzzy controller remain within a prescribed interval, ensuring consistent inference under varying excitation levels.

III. A comparative evaluation on a nonlinear four-story steel frame benchmark subjected to historical earthquake records (Kobe and Northridge), demonstrating improved reductions in key seismic response indices (e.g., peak-to-peak displacement/drift, control force, and control energy) relative to Type-II Fuzzy-PID and ANFIS-PID baselines.

The remainder of this paper is organized as follows: Section 2 details the dynamic system model of the four-story steel bending frame, including its nonlinear characteristics. Section 3 discusses the discretization of the system equations using the 4th-Order Runge-Kutta method. Section 4 presents the design of the proposed 2LT2-FLC, along with comparative analyses of Type-II Fuzzy-PID and ANFIS-PID controllers. Section 5 defines the cost function used for performance evaluation. Section 6 provides the results of the controller tests under Kobe and Northridge earthquakes, highlighting the effectiveness of the proposed method. Finally, Section 7 concludes the study, summarizes key findings, and suggests directions for future research.

2 Dynamic system

The structure considered in this study is a three-span, four-story steel frame with a total height of 12 m (3 m per story) and a total span length of 6 m. For control design and real-time simulation, the lateral dynamics are represented by an equivalent four-degree-of-freedom shear-building model, in which each floor has one lateral translational degree of freedom. Accordingly, the displacement, velocity, and acceleration vectors are defined as $d(t) \in R^4$, $\dot{d}(t) \in R^4$, and $\ddot{d}(t) \in R^4$, respectively. The dynamic response under seismic excitation is governed by the nonlinear equation of motion in Eq 1 consistent with the modeling approach reported in [6, 12, 17]

$$M\ddot{d} + C\dot{d} + Kd + F_{\text{nonlin,stiff}} + F_{\text{nonlin,damp}} = F_d + F_u, \tag{1}$$

where the dynamic model of the four-story steel bending frame defines the floor acceleration vector as $(\ddot{d})$, the floor velocity vector as $(\dot{d})$ or (v), and the floor displacement vector as (d). The external earthquake force is represented by the vector (F_d), while the control force vector is denoted as (F_u). Additionally, the model includes a cubic stiffness coefficient, (k_{cubic}), and a nonlinear damping force, $(F_{nonlin,damp})$. Eq 2 provide the formulations for calculating the nonlinear parameters of the steel bending frame model. Specifically, these equations define the relationships for determining the cubic stiffness coefficient, (k_{cubic}), and the nonlinear damping coefficient, $(F_{nonlin,damp})$, which govern the nonlinear behavior of the system under dynamic loading conditions.

$$\begin{cases} F_{\text{nonlin,stiff}} = k_{\text{cubic}} \cdot d^{\circ 3} \\ F_{\text{nonlin,damp}} = c_{\text{nonlin}} \cdot \left(|\dot{d}| \circ \dot{d}\right) \end{cases}. \tag{2}$$

The cubic stiffness term accounts for geometric hardening effects that arise in steel frames under large lateral displacements, while the nonlinear damping term models velocity-dependent energy dissipation that exceeds the capacity of linear viscous damping. These forms are commonly used as simplified representations of nonlinear structural behavior, and their coefficients have been selected to ensure that the free vibration response of the model reproduces the target damping ratio. Eq 3, m_x denotes the mass of the $x-th$ floor, $(I_b)_z$ represents the moment of inertia of the $z-th$

beam, and h_y indicates the height of the $y-th$ column. Additionally, (E) signifies the modulus of elasticity of the materials used in the structure. The matrices (Q) and (R) account for the influence of rotational degrees of freedom on the lateral stiffness of the building frame.

$$[K]=\begin{bmatrix} \sum_{i=1}^{8}\frac{12E(I_c)_i}{(h_i)^3} & -\sum_{i=5}^{8}\frac{12E(I_c)_i}{(h_i)^3} & 0 & 0 \\ -\sum_{i=5}^{8}\frac{12E(I_c)_i}{(h_i)^3} & \sum_{i=5}^{12}\frac{12E(I_c)_i}{(h_i)^3} & -\sum_{i=9}^{12}\frac{12E(I_c)_i}{(h_i)^3} & 0 \\ 0 & -\sum_{i=9}^{12}\frac{12E(I_c)_i}{(h_i)^3} & \sum_{i=9}^{16}\frac{12E(I_c)_i}{(h_i)^3} & -\sum_{i=13}^{16}\frac{12E(I_c)_i}{(h_i)^3} \\ 0 & 0 & -\sum_{i=13}^{16}\frac{12E(I_c)_i}{(h_i)^3} & \sum_{i=13}^{16}\frac{12E(I_c)_i}{(h_i)^3} \end{bmatrix}-[R][Q]^{-1}[R]^T, \tag{3}$$

$$[M]=\begin{bmatrix} m_1 & 0 & 0 & 0 \\ 0 & m_2 & 0 & 0 \\ 0 & 0 & m_3 & 0 \\ 0 & 0 & 0 & m_4 \end{bmatrix}.$$

To construct the classical damping matrix, the Caughey series damping model is adopted. In this approach, the damping matrix is expressed as a polynomial series of the matrix product $[M]^{-1}[K]$, as follows (Eq 4):

$$[c]_{Classical}=[M]\sum_{\tau=0}^{3}\alpha_\tau\left[[M]^{-1}[K]\right]^\tau. \tag{4}$$

The coefficients α_τ are selected such that the resulting modal damping ratios match the target values within the frequency range of interest.

Using Eq 5, we write 1 in the form of a state space equation. This model incorporates eight state-space variables, comprising four variables for floor displacement and four for floor velocity ($\zeta=[\zeta_{11},\zeta_{12},\zeta_{21},\zeta_{22},\zeta_{31},\zeta_{32},\zeta_{41},\zeta_{42}]^T=[v_1,d_1,v_2,d_2,v_3,d_3,v_4,d_4]^T$).

$$\begin{cases}\zeta_1=\ d\\ \zeta_2=\dot{d}\end{cases} \tag{5}$$

The form of the system's state space can be seen in Eq 6.

$$\begin{cases}\ \ \dot{\zeta_1}=\ d\\ M\dot{\zeta_2}=F_d+F_u-\ C\zeta_2-K\zeta_1-F_{\text{nonlin,stiff}}-F_{\text{nonlin,damp}}\end{cases} \tag{6}$$

Since natural frequency of structure is considered 1 Hz, the values of the matrices M, K and C are computed as bellows to meet this condition:

$$M=\begin{bmatrix} 4860 & 0 & 0 & 0 \\ 0 & 4860 & 0 & 0 \\ 0 & 0 & 4860 & 0 \\ 0 & 0 & 0 & 4860 \end{bmatrix}.$$

$$K=\begin{bmatrix} 29439009.8085361 & -15348279.4433451 & 4028460.5561258 & -592529.358945492 \\ -15348279.4433451 & 18726715.9553859 & -10950529.8230466 & 2405960.5986393 \\ 4028460.5561258 & -10950529.8230466 & 14182822.6575606 & -6353765.2997453 \\ -592529.358945492 & 2405960.5986393 & -6353765.2997453 & 4406445.14750445 \end{bmatrix}.$$

$$C=\begin{bmatrix} 35865.89398931 & -11961.6893230314 & 1098.30906826684 & -291.943097671596 \\ -11961.6893230314 & 25489.6989618342 & -10822.851428698 & 421.328563517596 \\ 1098.30906826683 & -10822.851428698 & 22117.7806787493 & -9041.49120151557 \\ -291.943097671597 & 421.328563517596 & -9041.49120151557 & 11495.3000174384 \end{bmatrix}.$$

3 Variable time-steps for model discretization

Given that the data we use is discrete, this section discusses the method of discretizing the equations of the system used.

3.1 4th-order Runge-Kutta (RK4) method

The fourth-order Runge-Kutta method, commonly referred to as RK4, is an explicit iterative method developed around 1900 by German mathematicians Carl Runge and Wilhelm Kutta [6]. The Runge-Kutta 4th-order (RK4) method is a widely used numerical technique for solving ordinary differential equations (ODEs) with high accuracy. Given an ODE of the form (Eq 7):

$$\frac{dy}{dt} = f(t, y), \quad y(t0) = y0. \tag{7}$$

The RK4 method approximates the solution at discrete time steps $t_{n+1} = t_n + h$ via intermediate calculations:

3.2 Slope estimation

Initially, the slopes were calculated using Eq 8.

$$\begin{aligned} K_1 &= hf(t_n, y_n), \\ K_2 &= hf(t_n + \frac{h}{2}, y_n + \frac{K_1}{2}), \\ K_3 &= hf(t_n + \frac{h}{2}, y_n + \frac{K_2}{2}), \\ K_4 &= hf(t_n + h, y_n + K_3). \end{aligned} \tag{8}$$

3.2.1 Solution update

The responses were then updated using Eq 9.

$$y_{n+1} = y_n + \frac{1}{6}(K_1 + 2K_2 + 2K_3 + K_4). \tag{9}$$

3.3 Discretization of system equations

Using the change of variable mentioned in Eq 5, 6 was written. By multiplying the inverse of matrix M on both sides of Eq 6, Eq 10 appears.

$$\begin{aligned} &\begin{cases} \dot{\zeta_1} = d \\ M\dot{\zeta_2} = F_d + F_u - C\zeta_2 - K\zeta_1 - F_{\text{nonlin,stiff}} - F_{\text{nonlin,damp}} \end{cases} \\ &\Rightarrow \quad \dot{\zeta_2} = M^{-1}(F_d + F_u - C\zeta_2 - K\zeta_1 - F_{\text{nonlin,stiff}} - F_{\text{nonlin,damp}}). \end{aligned} \tag{10}$$

According to the discretization method, the discretized equations will be in the following form (Eq 11):

$$\begin{aligned} K_1 &= f(t_n, \zeta_n) \\ K_1^{(1)} &= \zeta_2^{(n)} \\ K_1^{(2)} &= M^{-1}\left(F_d^{(n)} + F_u^{(n)} - C\zeta_2^{(n)} - K\zeta_1^{(n)} - F_{\text{nonlin,stiff}}\left(\zeta_1^{(n)}\right) - F_{\text{nonlin,damp}}\left(\zeta_2^{(n)}\right)\right) \\ K_2 &= f\left(t_n + \frac{h}{2}, \zeta_n + \frac{h}{2}K_1\right) \\ K_2^{(1)} &= \zeta_2^{(n)} + \frac{h}{2}K_1^{(2)} \\ K_2^{(2)} &= M^{-1}\left(F_d^{\left(n+\frac{h}{2}\right)} + F_u^{\left(n+\frac{h}{2}\right)} - C\left(\zeta_2^{\left(n+\frac{h}{2}\right)} + \frac{h}{2}K_1^{(2)}\right)\right. \end{aligned}$$

$$
\begin{aligned}
&-K\left(\zeta_1^{\left(n+\frac{h}{2}\right)}+\frac{h}{2}K_1^{(1)}\right)-F_{\text{nonlin,stiff}}\left(\zeta_1^{\left(n+\frac{h}{2}\right)}+\frac{h}{2}K_1^{(1)}\right)\\
&-F_{\text{nonlin,damp}}\left(\zeta_2^{\left(n+\frac{h}{2}\right)}+\frac{h}{2}K_1^{(2)}\right)\Big)\\
K_3 &= f\left(t_n+\frac{h}{2},\zeta_n+\frac{h}{2}K_2\right)\\
K_3^{(1)} &= \zeta_2^{(n)}+\frac{h}{2}K_2^{(2)}\\
K_3^{(2)} &= M^{-1}\left(F_d^{\left(n+\frac{h}{2}\right)}+F_u^{\left(n+\frac{h}{2}\right)}-C\left(\zeta_2^{\left(n+\frac{h}{2}\right)}+\frac{h}{2}K_2^{(2)}\right)\right.\\
&-K\left(\zeta_1^{\left(n+\frac{h}{2}\right)}+\frac{h}{2}K_2^{(1)}\right)-F_{\text{nonlin,stiff}}\left(\zeta_1^{\left(n+\frac{h}{2}\right)}+\frac{h}{2}K_2^{(1)}\right)\\
&-F_{\text{nonlin,damp}}\left(\zeta_2^{\left(n+\frac{h}{2}\right)}+\frac{h}{2}K_2^{(2)}\right)\Big)\\
K_4 &= f(t_n+h,\zeta_n+hK_3)\\
K_4^{(1)} &= \zeta_2^{(n)}+hK_3^{(2)}\\
K_4^{(2)} &= M^{-1}\left(F_d^{(n+h)}+F_u^{(n+h)}-C\left(\zeta_2^{(n+h)}+hK_3^{(2)}\right)-K\left(\zeta_1^{(n+h)}+hK_3^{(1)}\right)\right.\\
&-F_{\text{nonlin,stiff}}\left(\zeta_1^{(n+h)}+hK_3^{(1)}\right)-F_{\text{nonlin,damp}}\left(\zeta_2^{(n+h)}+hK_3^{(2)}\right)\Big)
\end{aligned}
$$

Update the state:

$$
\begin{aligned}
\zeta_1^{(n+1)} &= \zeta_1^{(n)}+\frac{h}{6}\left(K_1^{(1)}+2K_2^{(1)}+2K_3^{(1)}+K_4^{(1)}\right)\\
\zeta_2^{(n+1)} &= \zeta_2^{(n)}\frac{h}{6}\left(K_1^{(2)}+2K_2^{(2)}+2K_3^{(2)}+K_4^{(2)}\right).
\end{aligned}
\tag{11}
$$

4 Controller design

In this study, we investigate the performance of the proposed two-layer interval Type-II fuzzy controller (2LT2-FLC) for mitigating earthquake-induced vibrations in a four-story building. To provide a fair benchmark, we compare it with two widely used PID-based intelligent controllers: (i) a Type-II Fuzzy-PID controller and (ii) an ANFIS-PID controller. It is important to clarify that, although all controllers generate the control force online during simulation, the baseline controllers require offline procedures: the Fuzzy-PID uses offline optimization to tune the mapping coefficients, and the ANFIS-PID relies on offline training using recorded input–output data. In contrast, the proposed 2LT2-FLC performs online input normalization through its inner adaptive fuzzy layer without requiring offline optimization or data-driven training.

4.1 Type-II fuzzy-PID controller

4.1 Type-II Fuzzy-PID Controller

A Type-II Fuzzy-PID controller [22] was first designed as a baseline. The controller uses a single interval Type-II fuzzy inference system (FIS) to generate three tuning signals (($K_p^{'}$), ($K_d^{'}$), and (α)) from two inputs: the normalized displacement error e(t) and its derivative de(t), measured from the second floor. In this study, e(t) is defined with respect to a zero reference (i.e., vibration suppression), and both $e(t)$ and $de(t)$ are normalized to a fixed range (e.g., $[-1,\ 1]$) before entering the FIS to ensure consistent membership-function activation.

The fuzzy outputs are then mapped to the PID gains using Eq. (12):

$$
\begin{aligned}
K_p &= \lambda_1 K_p^{'}+\lambda_2,\\
K_d &= \lambda_3 K_d^{'}+\lambda_4,\\
K_i &= {K_p}^2/(\alpha K_d),
\end{aligned}
\tag{12}
$$

where λ_1, λ_2, λ_3, and λ_4 are constant mapping coefficients. These coefficients are tuned offline using the Chaos Game Optimization (CGO) algorithm [16] prior to the earthquake simulations (30 iterations with an initial population of 30 seeds). To avoid ill-conditioned integral gains, α and K_d are constrained to remain strictly positive during tuning. Table 1 also refers to the presentation of the rules used in the fuzzy system. It includes 49 rules.

Table 1: Fuzzy-PID rules

IF e is NB AND de is NB THEN $K_p^{'}$ *is Big,* $K_d^{'}$ *is Small,* α *is 2*
IF e is NB AND de is NM THEN $K_p^{'}$ *is Big,* $K_d^{'}$ *is Small,* α *is 2*
⋮
IF e is PB AND de is PB THEN $K_p^{'}$ *is Big,* $K_d^{'}$ *is Small,* α *is 2*

4.2 ANFIS-PID controller

The ANFIS-PID controller utilizes three Adaptive Neuro-Fuzzy Inference System models to dynamically compute the gains ($K_p^{'}$), ($K_d^{'}$), and (α). The inputs to each ANFIS model are the normalized displacement error and its derivative. A total of 18,190 data sets were stored for training ANFIS, of which 70% were used for training, 15% for validation, and 15% for testing. Fig 1 shows one of the structures of a fuzzy neural system, and as can be seen, in this structure we have 8 rules, and in total we have 24 rules, and like Fuzzy-PID we used 30 iterations and an initial population of 30 seeds.

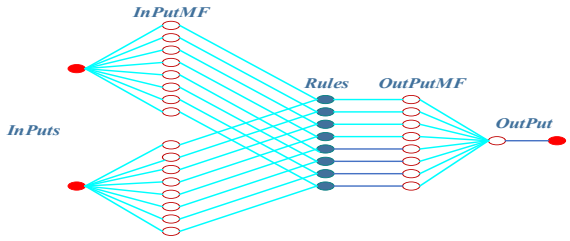

Fig 1 The ANFIS training structure

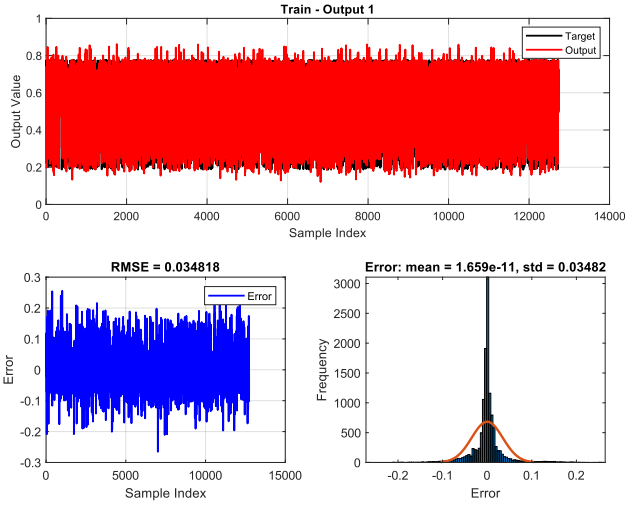

Fig 2 First ANFIS training specifications

The trained ANFIS model demonstrated strong predictive accuracy across 12,733 samples, achieving an RMSE of 0.0348 with errors tightly clustered near zero ($mean : \sim 10^{-11}$, $SD :$ 0.0348). While occasional deviations up to ± 0.3 highlighted challenges in handling rapid data shifts, the overall unbiased error distribution confirms reliable generalization.

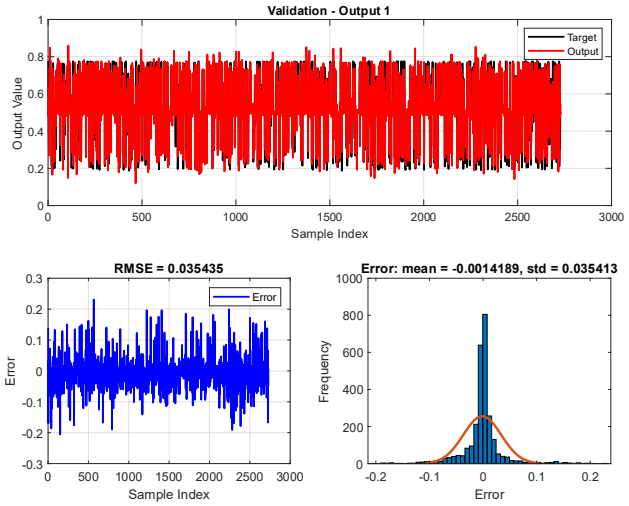

Fig 3 First ANFIS validation specifications

Validation of the ANFIS model on Output 1 confirmed robust predictive performance, with predictions closely aligning with target values across 2729 samples ($RMSE:\ 0.0354$). While most errors were tightly distributed ($SD:\ 0.0354$), occasional deviations up to ± 0.3 revealed challenges during abrupt data shifts. A slight mean error (-0.0142) indicated minimal systematic underprediction, but the near-normal error spread affirmed the model's reliability for regression and classification tasks.

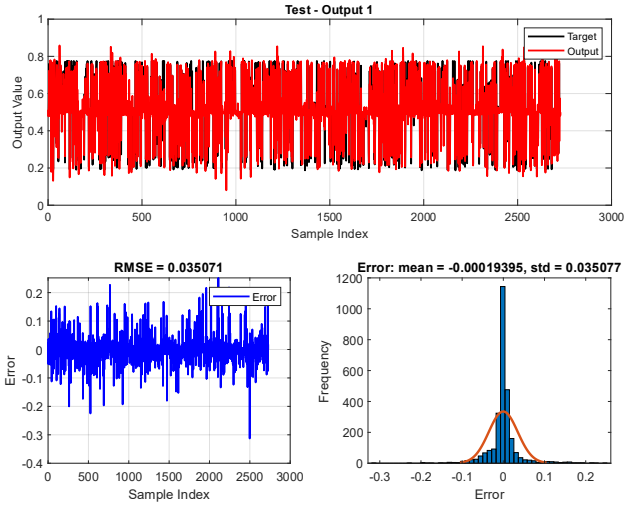

Fig 4 First ANFIS test specifications

Testing of the ANFIS model on Output 1 demonstrated strong predictive accuracy, with outputs closely matching targets across 2727 samples ($RMSE:\ 0.0351$). While most errors followed a near-normal distribution ($mean:\ -0.0019,\ SD:\ 0.0351$), occasional deviations up to ± 0.4 highlighted residual sensitivity to outliers and abrupt data variations. The negligible bias and tight error spread confirm the model's reliability for regression and classification applications

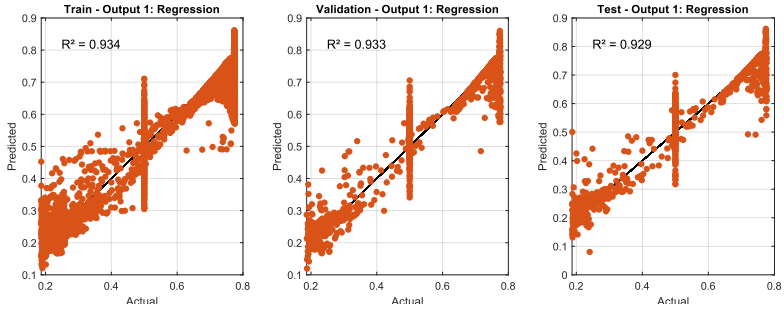

Fig 5 Regression diagram of training, validation and testing of the first ANFIS

The ANFIS network achieved consistent predictive accuracy across all phases for Output 1, with R^2 values of 0.934 (training), 0.933 (validation), and 0.929 (testing). While the marginal performance decline during testing reveals slight generalization limitations, the model maintains strong regression capability. The Adaptive Neuro-Fuzzy Inference System (ANFIS) network's performance for Output 2, detailed in the Table 2, shows a robust training phase with an R^2 of 0.904 and an RMSE of 0.036769, indicating high accuracy. However, validation and testing phases reveal a decline in performance, with R^2 dropping to 0.824 and 0.698 respectively, and RMSE increasing to 0.063868.

Table 2: Characteristics of the second trained ANFIS

Phase	**RMSE**	R^2	**Mean Error**	**Std. Deviation of Error**
Training	0.036769	0.904	1.6692e-10	0.036771
Validation	0.049853	0.824	-0.00085928	0.049855
Testing	0.063868	0.698	-0.0054395	0.063877

The Adaptive Neuro-Fuzzy Inference System (ANFIS) network for Output 3, as outlined in the Table 3, maintains strong performance with R^2 values around 0.904 to 0.893 across training, validation, and testing phases. The RMSE values, ranging from 0.11071 to 0.12235, indicate a slight increase in error during testing. The near-zero mean error values reflect minimal bias, though the growing standard deviation highlights potential challenges in generalization.

Table 3: Characteristics of the third trained ANFIS

Phase	**RMSE**	R^2	**Mean Error**	**Std. Deviation of Error**
Training	0.11071	0.904	-3.6412e-10	0.11071
Validation	0.11176	0.903	-0.0045607	0.11169
Testing	0.12235	0.893	-0.0044082	0.12229

4.3 Proposed adaptive two-layer fuzzy controller

The idea of designing a two-layer adaptive fuzzy controller is that there is an external fixed IT2FLC and an internal adaptive IT2FLC. At each time interval, this internal fuzzy controller updates and sends gains as outputs. This gain, when multiplied by the inputs of the external fuzzy controller, causes the input values to the external fuzzy system to be in the correct range. Fig 6 shows the block diagram of the system used and the controllers.

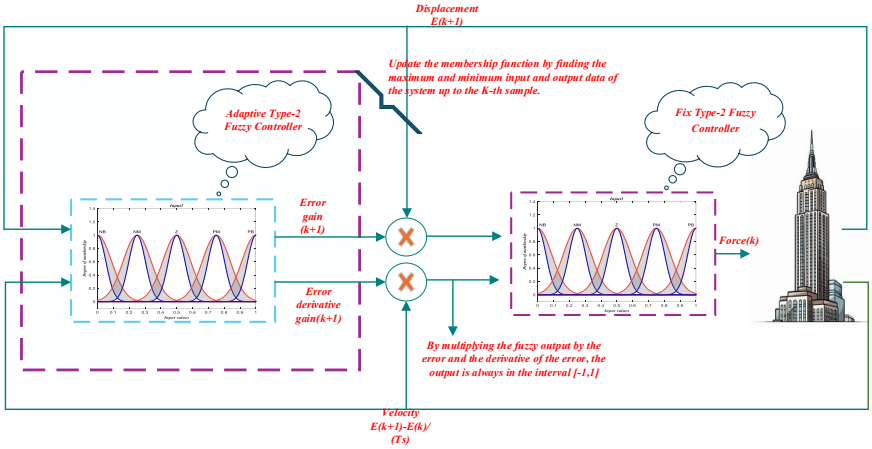

Fig 6 System block diagram

4.3.1 Internal Type- II fuzzy logic

The internal Type-II fuzzy system is designed with two inputs-second-stage displacement and second-stage velocity - and two outputs. These gains, which are the outputs of the internal Type-II fuzzy system, are used to adjust the input range of the external Type-II fuzzy system. Given the symmetry in the problem, we focus on the membership functions for the displacement gain output, without loss of generality. The membership functions for the velocity gain output are configured similarly. In the first step, all membership functions of the internal fuzzy system for inputs and outputs are defined as triangular. The locations of the triangular membership functions for the displacement input are specified in Table 4 (The membership functions of the second input of the internal type-II fuzzy (second-stage velocity input) are also defined in the same way). α and β are minimum and maximum of the second-floor displacement, respectively. The values α and β are updated as the running minimum and maximum over the entire history of the signal: $\alpha(k) = \min(\alpha(k-1), e(k))$ and $\beta(k) = \max(\beta(k-1), e(k))$. For initializing this algorithm, the smallest negative and positive values are considered at $k = 0$ as $\alpha(0) = -eps$ and $\beta(0) = +eps$

Also, the main range of membership functions for the input is $[\alpha\ \beta]$. It is important to mention that α is negative and β is positive and it is clear because the minimum and maximum of the second floor is negative and positive, respectively.

Table 4: Membership location of the first input functions for the internal fuzzy system

Membership Function number	Location of membership Function
(1) Negative-Big	$[1.5\alpha \quad \alpha \quad 0.5\alpha]$
(2) Negative-Normal	$[\alpha \quad 0.5\alpha \quad 0]$
(3) Zero	$[0.5\alpha \quad 0 \quad 0.5\beta]$
(4) Positive-Normal	$[0 \quad 0.5\beta \quad \beta]$
(5) Positive-Big	$[0.5\beta \quad \beta \quad 1.5\beta]$

For the output membership functions, the main domain is defined within the range $[1/\alpha\ 1/\beta]$, ensuring that the gain adjustments scale the external fuzzy system's inputs appropriately. Table 4 specifies the locations of the output membership functions.

Table 5: Internal Fuzzy rules

If the second-floor displacement is negative big and speed is negative big, then Output1 is negative big and Output2 is negative big
If the second-floor displacement is negative big and speed is negative normal, then Output1 is negative big and Output2 is negative normal
⋮

If the second-floor displacement is negative big and speed is negative big, then Output1 is negative big and Output2 is negative big
If the second-floor displacement is positive big and speed is positive big, then Output1 is positive big and Output2 is positive big

Table 6 presents some rules based on the internal fuzzy system. This system uses the displacement and velocity of the second floor as inputs.

Table 6: Membership location of the first output functions for the internal fuzzy system

Membership Function number	Location of membership Function
(1) Negative-Big	$[1.5\alpha^{-1} \quad \alpha^{-1} \quad 0.5 * \alpha^{-1}]$
(2) Negative-Normal	$[\alpha^{-1} \quad 0.5\alpha^{-1} \quad 0]$
(3) Zero	$[0.5\alpha^{-1} \quad 0 \quad 0.5\beta^{-1}]$
(4) Positive-Normal	$[0 \quad 0.5\beta^{-1} \quad \beta^{-1}]$
(5) Positive-Big	$[0.5\beta^{-1} \quad \beta^{-1} \quad 1.5\beta^{-1}]$

Given that the output of the internal fuzzy system is defined within a dynamic range, we ensure that it appropriately scales the inputs of the external fuzzy system.

4.3.2 External Type-II fuzzy logic

Next, we examine the external Type-II fuzzy system, which is designed to generate a control force. The membership functions of this fuzzy system are defined within a fixed range of [-1, 1]. By multiplying the gains derived from the internal Type-II fuzzy system with the inputs to the external fuzzy system, the resulting input values are constrained to remain within [-1, 1], ensuring stable and bounded control outputs. Table 7 presents the external fuzzy controller's rule base, defining the mapping of inputs to control outputs. In total, there are 25 rules for the external type-II fuzzy set, which are derived from 2 inputs, displacement and velocity of the second floor, each input having 5 membership functions. The number of output membership functions is also 5. The membership functions of the fuzzy controller are also entirely triangular, and the input and output membership functions are all defined in the range $[-1, 1]$.

The external IT2FLC receives the normalized inputs $\xi(t) = [\overline{\overline{e}}(t), \ d\overline{\overline{e}}(t)]^\top$, where $\overline{\overline{e}}(t) = |g_e|e(t)$ and $d\overline{\overline{e}}(t) = |g_{de}|de(t)$, and by design $\xi(t) \in [-1, 1]^2$ for all t.

Table 7: External Fuzzy rules

If the second-floor displacement is negative big and speed is negative big, then force is positive big
If the second-floor displacement is negative big and speed is negative normal, then force is positive big
⋮
If the second-floor displacement is positive big and speed is positive big, then force is negative big

4.3.3 Bounding the scaled input in the two-layer Type-II adaptive fuzzy logic controller

In the proposed Two-Layer Type-II Adaptive Fuzzy Logic Controller (2LT2-FLC), the inner adaptive layer generates gains that dynamically scale the inputs to the outer fuzzy layer, ensuring robust real-time control of seismic responses. A critical design requirement is that the scaled input, formed by multiplying the defuzzified gain g from the inner layer by the current input x, remains within the normalized range $[-1, 1]$. This section presents formal proof demonstrating that, under the specified controller architecture, $-1 \leq g \cdot x \leq 1$, thereby maintaining compatibility with the outer layer's fixed membership functions defined over $[-1, 1]$. The inner layer employs an interval Type-2 fuzzy system (IT2FS) with M rules, where the antecedents are interval Type-2 membership functions with lower bound $\underline{\mu}_{A_i^j}(x_j)$ and upper bound $\overline{\mu}_{A_i^j}(x_j)$ for each input x_j (error (e) and its derivative (de)). The consequents are crisp centers z_i, designed based on the adaptive parameters a (running minimum of the input history, $\alpha \leq 0$) and β (running maximum, $\beta \geq 0$), such that $z_i \in [1/\beta, \ 1/|\alpha|]$ The current input x is constrained to $[\alpha, \ \beta]$ by the controller's history-tracking mechanism. The proof proceeds as follows. First, the firing interval for rule i is computed as:

$$\underline{f}_i = \prod_{j=1}^{p} \underline{\mu}_{A_i^j}(x_j), \quad \overline{f}_i = \prod_{j=1}^{p} \overline{\mu}_{A_i^j}(x_j),$$

where $0 \leq \underline{f}_i \leq \overline{f}_i \leq 1$ due to the product of membership values in $[0, 1]$. Type-reduction is performed using the Karnik-Mendel (KM) algorithm, yielding the interval $[y_l,\ y_r]$, where:

$$y_l = \frac{\sum_{i=1}^{L} \overline{f}_i z_i + \sum_{i=L+1}^{n} \underline{f}_i z_i}{\sum_{i=1}^{L} \overline{f}_i + \sum_{i=L+1}^{n} \underline{f}_i}, \quad y_r = \frac{\sum_{i=1}^{R} \underline{f}_i z_i + \sum_{i=R+1}^{n} \overline{f}_i z_i}{\sum_{i=1}^{R} \underline{f}_i + \sum_{i=R+1}^{n} \overline{f}_i}.$$

Here, L and R are switch points determined iteratively, ensuring convergence to the optimal bounds within the consequent range. The defuzzified gain is then $g = (y_l + \ y_r)/2$.

Since y_l and y_r are weighted averages, define the weights for y_l as $\omega_i^l = \ \overline{f}_i/D_l$ for $i \ \ L$ and $\omega_i^l = \ \overline{f}_i/D_l$ for $i \ > \ L$, with $D_l = \sum_{i=1}^{L} \overline{f}_i + \sum_{i=L+1}^{n} \underline{f}_i$. Given that $\underline{f}_i$, $\overline{f}_i$ and $\sum \omega_i^l$, it follows that:

$$y_l = \sum_{i=1}^{M} \omega_i^l z_i.$$

Where $\min_i \ z_i \leq y_l \leq \max_i \ z_i$. Similarly, satisfies the same bond. Thus, $g \ \ [min\ zi\ ,\ max\ zi\ ]$.

The consequent centers z_i are strategically placed to reflect the inverse of the input range. For $x \approx \beta$ (*large positive input*), rules with $z_i \approx \beta^{-1}$ dominate, yielding $g \approx \beta^{-1}$, so $g.x \approx \beta^{-1}$. $\beta = 1$. For $x \approx \alpha$ (*large negative input*), rules with $z_i \approx |\alpha|^{-1}$ dominate, yielding $g \approx |\alpha|^{-1}$, so $g.x \approx |\alpha|^{-1}$. $\alpha = -1$. For x near zero, g blends toward the average of the range, and $|g.x| \ll 1$ due to the small magnitude of x. The fuzzy rule base, designed with linguistic terms (e.g., NB, Z, PB) and tuned via expert knowledge, ensures that intermediate x values result in $|g.x| \ll 1$, as the fired z_i adaptively scale g to match the input magnitude.

4.3.4 Stability and feasibility analysis of the proposed two-layer IT2-FLC

In this subsection, the stability and practical feasibility of the proposed two-layer interval type-II fuzzy logic controller (2LT2-FLC) are analyzed. The nonlinear structural system equipped with the ATMD can be written as (We rewrote Eq 1 in another format.):

$$M\ddot{d}(t) + C\dot{d}(t) + Kd(t) + F_s\left(d(t)\right) + F_d\left(d(t),\ \dot{d}(t)\right) = B_u u(t) + B_g a_g(t). \tag{13}$$

Where $F_s(\cdot)$ represents the nonlinear restoring forces; $F_d(\cdot,\cdot)$ denotes the nonlinear damping forces; $u(t)$ is the ATMD control force; and $a_g(t)$ is the ground acceleration.

The following standard assumptions are adopted, which are consistent with the structural model used in this study:

A1. The mass and stiffness matrices are symmetric positive definite.

A2. The viscous damping matrix is symmetric positive definite, $C = C^\top \succ 0$; hence $\dot{d}^\top C\dot{d} \geq \lambda_{\min}(C) \parallel \dot{d} \parallel^2$ for all $\dot{d}$, where $\lambda_{\min}(C) > 0$ denotes the smallest eigenvalue of C.

A3. The nonlinear restoring forces derive from a non-negative potential function.

$$F_s(d) = \frac{\partial \Psi(d)}{\partial d}, \Psi(d) \geq 0, \forall d \in \mathbb{R}^n, \tag{14}$$

where, for instance, $\Psi(d)$ contains the cubic stiffness energy terms.

A4. The nonlinear damping forces are dissipative:

$$\dot{d}^\top F_d\left(d, \dot{d}\right) \geq 0 \qquad \forall (d, \dot{d}) \in \mathbb{R}^n \times \mathbb{R}^n.$$

A5. The ground acceleration is bounded,

$$\parallel a_g(t) \parallel \leq \bar{a}_g < \infty, \quad \forall t \geq 0.$$

We introduce the state vector

$$x(t) = \left[\ \begin{matrix} d(t) \\ \dot{d}(t) \end{matrix}\ \right] \in \mathbb{R}^{2n}.$$

Lyapunov function:

To analyze the closed-loop behavior, we consider the Lyapunov candidate

$$V(x) = \frac{1}{2}\dot{d}^\top M\dot{d} + \frac{1}{2}d^\top Kd + \Psi(d). \tag{15}$$

By Assumptions A1 and A3, there exist positive constants $\underline{c}, \bar{c} > 0$ such that

$$\underline{c} \parallel x \parallel^2 \leq V(x) \leq \bar{c} \parallel x \parallel^2, \tag{16}$$

for all $x \in \mathbb{R}^{2n}$; hence $V(x)$ is positive definite and radially unbounded.
The time derivative of Valong the trajectories of (Eq 13) is:

$$\dot{V} = \dot{d}^\top M\ddot{d} + d^\top K\dot{d} + \frac{\partial\Psi}{\partial d}^\top \dot{d}. \tag{17}$$

Substituting (Eq 13) into $M\ddot{d}$ yields:

$$\dot{V} = \dot{d}^\top(-C\dot{d} - Kd - F_s(d) - F_d(d,\dot{d}) + B_u u + B_g a_g) + d^\top K\dot{d} + \frac{\partial\Psi}{\partial d}^\top \dot{d}. \tag{18}$$

Using the symmetry of K and Assumption A3, we obtain $d^\top K\dot{d} = \dot{d}^\top Kd$ and $F_s(d) = \partial\Psi/\partial d$, so that

$$-\dot{d}^\top Kd + d^\top K\dot{d} = 0,$$
$$-\dot{d}^\top F_s(d) + \frac{\partial\Psi}{\partial d}^\top \dot{d} = 0.$$

Therefore, all stiffness-related terms cancel out and (Eq 18) simplifies to

$$\dot{V} = -\dot{d}^\top C\dot{d} - \dot{d}^\top F_s(d,\dot{d}) + \dot{d}^\top B_u u + \dot{d}^\top B_g a_g. \tag{19}$$

Bounding the Lyapunov:

From Assumption A2, $C > 0$ implies

$$\dot{d}^\top C\dot{d} \geq \lambda_{\min}(C) \ \parallel \dot{d} \parallel^2,$$

so that

$$-\dot{d}^\top C\dot{d} \leq -c_1 \parallel \dot{d} \parallel^2, \qquad c_1 := \lambda_{\min}(C) > 0. \tag{20}$$

Where c_1 is $\lambda_{\min}$. Assumption A4 guarantees $\dot{d}^\top F_d(d,\dot{d}) \geq 0$, hence

$$-\dot{d}^\top F_d(d,\dot{d}) \leq 0. \tag{21}$$

Using (Eq 20) – (Eq 21) in (Eq 19), we obtain

$$\dot{V} \leq -c_1 \parallel \dot{d} \parallel^2 + \dot{d}^\top B_u u + \dot{d}^\top B_g a_g. \tag{22}$$

The last two terms in (34) can be bounded using the Cauchy–Schwarz inequality and the induced matrix norm:

$$\begin{aligned} \mid \dot{d}^\top B_u u \mid &\leq \parallel \dot{d} \parallel \ \parallel B_u \parallel \ \mid u \mid, \\ \mid \dot{d}^\top B_g a_g \mid &\leq \parallel \dot{d} \parallel \ \parallel B_g \parallel \ \parallel a_g \parallel. \end{aligned} \tag{23}$$

Therefore,

$$\dot{V} \leq -c_1 \parallel \dot{d} \parallel^2 + \parallel \dot{d} \parallel \ \parallel B_u \parallel \ \mid u \mid + \parallel \dot{d} \parallel \ \parallel B_g \parallel \ \parallel a_g \parallel. \tag{24}$$

At this point, the specific structure of the proposed controller is used. The control force is generated by the 2LT2-FLC as

$$u(t) = \mathcal{F}(\bar{e}(t), \dot{\bar{e}}(t)), \tag{25}$$

where $\bar{e}(t)$ and $\dot{\bar{e}}(t)$ are the normalized displacement and velocity errors delivered by the inner adaptive IT2-FLC layer, and $\mathcal{F}(\cdot)$ denotes the mapping realized by the outer fixed IT2-FLC. As proven in Section 4.3.3, the inputs to the outer fuzzy controller satisfy

$$\bar{e}(t),\ \dot{\bar{e}}(t) \in [-1,1] \qquad \forall t, \tag{26}$$

so, the input vector $\xi(t) = [\bar{e}(t), \dot{\bar{e}}(t)]^\top$ belongs to the compact set $\Omega = [-1,1]^2$.

The outer IT2-FLC has a finite number of rules and singleton consequences; its type-reduction and defuzzification can be expressed as a continuous function of ξ on Ω. Hence there exists a constant $U_{\max} > 0$ such that

$$\mid u(t) \mid = \mid \mathcal{F}(\xi(t)) \mid \leq U_{\max}, \forall\ \xi(t) \in \Omega. \tag{27}$$

Using (Eq 27) together with Assumption A5 ($\parallel a_g(t) \parallel \leq \bar{a}_g$), inequality (Eq 24) becomes

$$\dot{V} \leq -c_1 \parallel \dot{d} \parallel^2 + \parallel \dot{d} \parallel (\parallel B_u \parallel U_{\max} + \parallel B_g \parallel \bar{a}_g). \tag{28}$$

Denote $c_2 = \parallel B_u \parallel U_{\max} + \parallel B_g \parallel \bar{a}_g$. Then

$$\dot{V} \leq -c_1 \parallel \dot{d} \parallel^2 + c_2 \parallel \dot{d} \parallel . \tag{29}$$

Since $\parallel \dot{d} \parallel^2$and $\parallel x \parallel^2$are equivalent up to positive constants (because $x = [d^\top, \dot{d}^\top]^\top$and V satisfies (Eq 16)), there exist $\alpha_1, \alpha_2 > 0$ such that

$$\dot{V}(x) \leq -\alpha_1 \parallel x \parallel^2 + \alpha_2 \parallel x \parallel . \tag{30}$$

Input-to-state stability and post-earthquake behavior:

Inequality (Eq 30) has the standard structure used in input-to-state stability (ISS) analysis. For sufficiently large $\parallel x \parallel$, the quadratic term $-\alpha_1 \parallel x \parallel^2$ dominates the linear term $\alpha_2 \parallel x \parallel$, implying that $\dot{V}(x)$ becomes negative and the state is driven toward a bounded region whose size depends on α_2, and hence on the bounds $U_{\max}$ and $\bar{a}_g$. Therefore, the closed-loop system is input-to-state stable with respect to the ground acceleration: for any bounded seismic excitation $a_g(t)$, the state $x(t)$ remains bounded for all $t \geq 0$.

After the end of the earthquake, i.e. when $a_g(t) \equiv 0$ for all $t \geq T_f$, the disturbance term (Eq 30) disappears. Under the standard assumption that the reference displacement is zero and that the fuzzy controller satisfies $u(t) \to 0$ as $x(t) \to 0$, the inequality (Eq 30) reduces, in a neighborhood of the origin, to

$$\dot{V}(x) \leq -\widetilde{\alpha}_1 \parallel x \parallel^2, \tag{31}$$

for some $\widetilde{\alpha}_1 > 0$. Classical Lyapunov theory then guarantees that the origin is an asymptotically stable equilibrium of the closed-loop system in the post-earthquake phase.

$$x(t) \to 0 \text{ as } t \to \infty.$$

Feasibility in real-time implementation:

A critical claim of this study is the real-time feasibility of the proposed 2LT2-FLC. To validate this, the computational burden of the control algorithm was evaluated in isolation from the plant simulation. The controller's code was executed on a standard laptop computer (Intel i7-9th Gen, 32 GB RAM) running MATLAB 2024a. The average time required to compute the control force for a single time step was found to be approximately 0.2 milliseconds (ms). This analysis was conducted using a sampling time of 0.02 seconds (50 Hz). The results demonstrate that the proposed controller utilizes only 1% of the available time per control cycle. This leaves a substantial 99% margin for essential ancillary processes such as data acquisition from sensors, signal filtering, communication with the actuator, and system safety checks.

5 Cost function

The proposed optimization framework evaluates controller performance using a weighted Mult objective cost function, combining key control metrics into a single scalar value. The total cost J is computed as:

$$J = \sum_i \varpi_i.(\frac{C_i}{C_{i,max}}). \tag{32}$$

Where C_i represents the raw cost components, $C_{i,max}$ their normalization bounds, and ω_i are weights. The normalized cost components are shown in Eq 33. The values ϖ_i are displayed in Table 8.

$$C_i = \varpi_1 \sum_{k=1}^{T} k\,|e(k)| + \varpi_2 \sum_{k=1}^{T} u(k)^2 + \varpi_3 |y_{ref} - y(k)|. \tag{33}$$

Where, T is the number of samples in the earthquake duration and y_{ref} is assumed to be zero, because it is the best possible value for a structure when the structure is vibration-free. Normalization ensures all cost components contribute equally to the optimization process by scaling them to a common range [0, 1], preventing larger-magnitude metrics from dominating the objective function. This improves optimization stability, enhances interpretability of results, and allows for more intuitive weight tuning when balancing competing performance criteria. By eliminating scale bias, normalization enables fair comparisons across different systems and control strategies.

Table 8: values of ϖ_i

ϖ_1	10	To minimize the integrated absolute error, ensuring overall response reduction.
ϖ_2	2.5	To penalize high control force and minimize energy consumption.
ϖ_3	12.5	To prioritize the minimization of peak displacement, which is most critical for preventing structural damage.

6 Result

Fig 7 illustrates the lateral displacement responses of the second and fourth floors under the Kobe earthquake excitation. As can be observed, the proposed 2LT2-FLC significantly reduces the response amplitudes: the peak-to-peak displacement is reduced by 49.44% on the second floor and 49.65% on the fourth floor, compared with the uncontrolled case. In addition, the settling (damping) time of the structure is shortened, indicating faster vibration suppression.

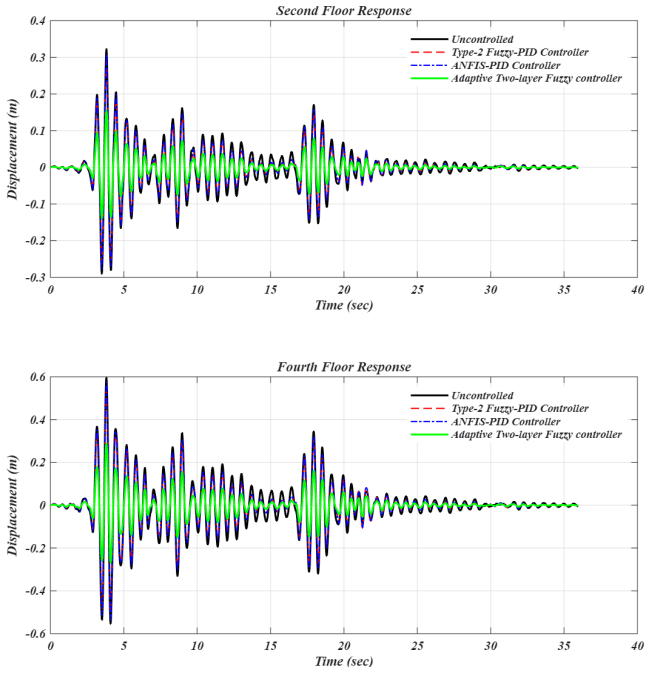

Fig 7 Structural displacement on the second and fourth floors due to the Kobe earthquake

Table 9 summarizes the controller performance under the Kobe earthquake excitation. The reported indices include: (i) the peak-to-peak interstory drift ratio of Story 2, (ii) the percentage reduction of this value relative to the uncontrolled structure, (iii) the displacement of all stories over the earthquake duration, and (iv) the cost function value for the optimized baseline controllers (Type-II Fuzzy-PID and ANFIS-PID).

The peak-to-peak interstory drift ratio of story i is computed from the relative displacement between two consecutive floors (Eq 34):

$$\begin{aligned} \Upsilon_i[k] &= (x_i[k] - \ x_{i-1}[k])/h_s \\ \Delta_i^{pp} &= \max_{1\le k\le K} \ \Upsilon_i[k] - \min_{1\le k\le K} \ \Upsilon_i[k]. \end{aligned} \tag{34}$$

Where $x_i[k]$ and h_s denote the lateral displacement and height story of floor i at time step k, and K is the total number of samples. The percentage reduction of the peak-to-peak drift compared to the uncontrolled structure is then given by Eq 35.

$$R_i = \frac{\Delta^{pp}_{i,\ uncontrolled} - \Delta^{pp}_{i,controlled}}{\Delta^{pp}_{i,\ uncontrolled}} \times 100. \tag{35}$$

The percentage reduction of this value compared to the uncontrolled case directly reflects the effectiveness of the controller. As shown, the proposed two-layer type-2 fuzzy controller achieves a substantially larger reduction in peak-to-peak drift than both the Fuzzy-PID and ANFIS-PID controllers, demonstrating its superior seismic performance. Equally important is the average displacement across all floors, which provides a comprehensive measure of the structural response by accounting for both large and small oscillations over the entire earthquake duration. This index captures the global vibration characteristics of the structure.

The average displacement of all floor's accounts for oscillations at every level of the structure during the entire earthquake duration (Eq 36):

$$\overline{x} = \frac{1}{NK} \sum_{i=1}^{N} \sum_{k=1}^{K} |x_i[k]|. \tag{36}$$

where N is the total number of floors.

Remark 6.1. *Since the uncontrolled case and the proposed 2LT2-FLC do not require any optimization procedure, the cost function value is not applicable and is therefore marked with "–". For the Type-II Fuzzy-PID and ANFIS-PID controllers, the reported cost corresponds to the optimization objective defined in Eq (33).*

Table 9: Controller performance evaluation criteria for reducing structural displacement due to the Kobe earthquake

Method				
	Uncontrolled	Type-II Fuzzy-PID	ANFIS-PID	2LT2 -FLC
peak-to-peak interstory drift ratio	0.5805	0.4837	0.5296	0.2892
Cost Function	–	156.4789	157.8931	–
Peak Reduction	–	16.6753%	8.7683%	50.1809%
Average Displacement	0.0286	0.0209	0.0221	0.0109

Fig 8 also shows the performance of this method compared to other methods. Again, this method has much better performance than other methods.

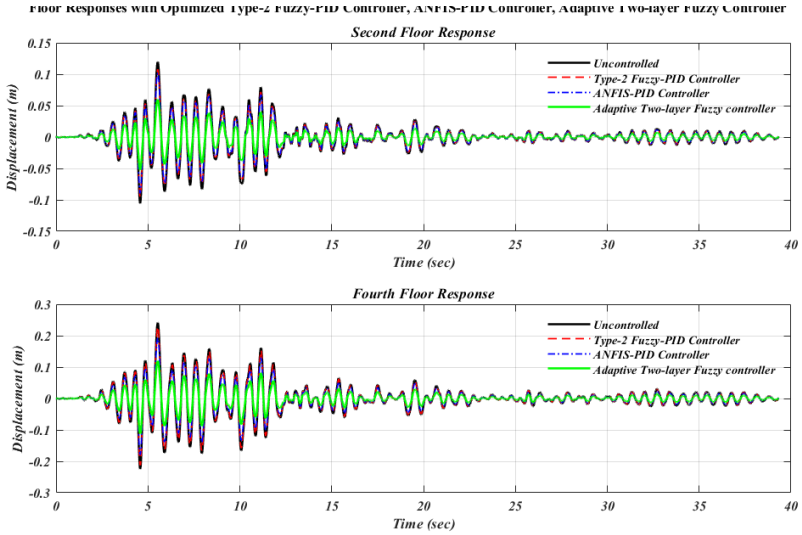

Fig 8 Structural displacement on the second and fourth floors due to the Northridge earthquake

Table 10 reports the controller performance indices under the Northridge earthquake excitation based on the second-story interstory drift ratio. The reported indices include: (i) the peak-to-peak interstory drift ratio of Story 2, (ii) the percentage reduction of this value relative to the uncontrolled structure, (iii) the average absolute displacement across all floors over the earthquake duration, and (iv) the cost function value for the optimized baseline controllers. As can be seen, the proposed Two-Layer Type-II Adaptive fuzzy method reduces the peak-to-peak interstory drift ratio of Story 2 by 47.6909% compared with the uncontrolled case.

Table 10: Controller performance evaluation criteria for reducing structural displacement due to the Northridge earthquake

Method				
	Uncontrolled	Type-II Fuzzy-PID	ANFIS-PID	2LT2 -FLC
peak-to-peak interstory drift ratio	0.2252	0.1999	0.2054	0.1178
Cost Function	–	164.3491	167.1436	–
Peak Reduction	–	11.2345%	8.7922%	47.6909%
Average Displacement	0.0137	0.0128	0.0131	0.0059

7 Conclusion

This paper presented a two-layer interval Type-II fuzzy logic controller (2LT2-FLC) for active seismic vibration mitigation of a nonlinear four-story building equipped with an ATMD. The proposed architecture combines an inner adaptive layer that performs online input normalization with an outer fixed IT2FLC that preserves an interpretable rule base. Simulation results under the Kobe and Northridge earthquake records indicate that the proposed method achieves larger reductions in peak-to-peak response measures compared with the Type-II Fuzzy-PID and ANFIS-PID baselines, while maintaining a low computational burden suitable for real-time implementation. Future work will focus on extending the approach to higher-dimensional structural models, refining the selection of normalization bounds/weights, and validating the method under additional ground motions and uncertainty scenarios.

References

[1] H. Aggumus, R. Guclu, *Hybrid experimental investigation of MR damper controlled tuned mass damper used for structures under earthquakes*, Journal of Soft Computing and Artificial Intelligence, **3**(1) (2022), 28-33. https://doi.org/10.55195/jscai.1122514

[2] C. O. Azeloglu, A. Sagirli, A. Edincliler, *Vibration mitigation of nonlinear crane system against earthquake excitations with the self-tuning fuzzy logic PID controller*, Nonlinear Dynamics, **84**(4) (2016), 1915-1928. https://doi.org/10.1007/s11071-016-2616-5

[3] M. Azizi, et al., *Upgraded whale optimization algorithm for fuzzy logic based vibration control of nonlinear steel structure*, Engineering Structures, **192** (2019), 53-70. https://doi.org/10.1016/j.engstruct.2019.05.007

[4] Y. Bigdeli, D. Kim, *Damping effects of the passive control devices on structural vibration control: TMD, TLC and TLCD for varying total masses*, KSCE Journal of Civil Engineering, **20**(1) (2016), 301-308. https://doi.org/10.1007/s12205-015-0365-5

[5] M. Bozorgvar, S. M. Zahrai, *Semi-active seismic control of buildings using MR damper and adaptive neural-fuzzy intelligent controller optimized with genetic algorithm*, Journal of Vibration and Control, **25**(2) (2018), 273-285. https://doi.org/10.1177/1077546318774502

[6] J. C. Butcher, G. Wanner, *Runge-Kutta methods: Some historical notes*, Applied Numerical Mathematics, **22**(1-3) (1996), 113-151. https://doi.org/10.1016/S0168-9274(96)00048-7

[7] S. Das, et al., *A novel fractional order fuzzy PID controller and its optimal time domain tuning based on integral performance indices*, Engineering Applications of Artificial Intelligence, **25**(2) (2012), 430-442. https://doi.org/10.1016/j.engappai.2011.10.004

[8] S. Das, I. Pan, S. Das, *Performance comparison of optimal fractional order hybrid fuzzy PID controllers for handling oscillatory fractional order processes with dead time*, ISA Transactions, **52**(4) (2013), 550-566. https://doi.org/10.1016/j.isatra.2013.03.004

[9] F. Fathi, A. K. Ashtiani, M. R. K. Ardakani, M. Pourgholi, A. H. Fesahat, M. Gholinia. *Adaptive fuzzy control of structures using slime Mould algorithm for earthquake vibration reduction*, in 2025 11th International Conference on Control, Instrumentation and Automation (ICCIA), 2025. https://doi.org/10.1109/ICCIA69223.2025.11285952

[10] S. Golnargesi, H. Shariatmadar, H. M. Razavi, *Seismic control of buildings with active tuned mass damper through interval type-2 fuzzy logic controller including soil–structure interaction*, Asian Journal of Civil Engineering, **19**(2) (2018), 177-188. https://doi.org/10.1007/s42107-018-0016-5

[11] R. Guclu, H. Yazici, *Vibration control of a structure with ATMD against earthquake using fuzzy logic controllers*, Journal of Sound and Vibration, **318**(1-2) (2008), 36-49. https://doi.org/10.1016/j.jsv.2008.03.058

[12] M. S. Jaballah, S. Harzallah, B. Nail, *Vibration control and seismic damages reduction for structural buildings based on optimal fractional-order controller and a graphical user interface development*, Journal of Vibration Engineering and Technologies, **11**(8) (2023), 4349-4370. https://doi.org/10.1007/s42417-022-00819-y

[13] S. Pourzeynali, H. H. Lavasani, A. Modarayi, *Active control of high rise building structures using fuzzy logic and genetic algorithms*, Engineering Structures, **29**(3) (2007), 346-357. https://doi.org/10.1016/j.engstruct.2006.04.015

[14] M. Ramirez-Neria, J. Morales-Valdez, W. Yu, *Active vibration control of building structure using active disturbance rejection control*, Journal of Vibration and Control, **28**(17-18) (2021), 2171-2186. https://doi.org/10.1177/10775463211009377

[15] Y. Shen, A. Homaifar, D. Chen. *Vibration control of flexible structures using fuzzy logic and genetic algorithms*, in Proceedings of the 2000 American Control Conference. ACC (IEEE Cat. No. 00CH36334), IEEE, 2000. https://doi.org/10.1109/ACC.2000.878940

[16] S. Talatahari, M. Azizi, *Chaos game optimization: A novel metaheuristic algorithm*, Artificial Intelligence Review, **54**(2) (2020), 917-1004. https://doi.org/10.1007/s10462-020-09867-w

[17] S. Thenozhi, W. Yu, *Advances in modeling and vibration control of building structures*, Annual Reviews in Control, **37**(2) (2013), 346-364. https://doi.org/10.1016/j.arcontrol.2013.09.012

[18] R. S. Tomar, M. F. Qureshi, S. K. Shrivastava, *Development of ANFIS controller and PID controller for seismic vibration control of structural system*, International Journal of Advanced Engineering Research and Science, **3**(11) (2016), 138-150. https://doi.org/10.22161/ijaers/3.11.24

[19] A. P. Wang, Y. H. Lin, *Vibration control of a tall building subjected to earthquake excitation*, Journal of Sound and Vibration, **299**(4-5) (2007), 757-773. https://doi.org/10.1016/j.jsv.2006.07.016

[20] S. Yaghoobi, S. Fadali, G. Pekcan, *Performance-based active controller design for nonlinear structures using modified black hole optimization*, Journal of Vibration and Control, **30**(3-4) (2023), 711-726. https://doi.org/10.1177/10775463221150053

[21] J. P. Zand, J. Sabouri, J. Katebi, M. Nouri, *A new time-domain robust anti-windup PID control scheme for vibration suppression of building structure*, Engineering Structures, **244** (2021), 112819. https://doi.org/10.1016/j.engstruct.2021.112819

[22] Z. Y. Zhao, M. Tomizuka, S. Isaka, *Fuzzy gain scheduling of PID controllers*, IEEE Transactions on Systems, Man, and Cybernetics, **23**(5) (1993), 1392-1398. https://doi.org/10.1109/21.260670